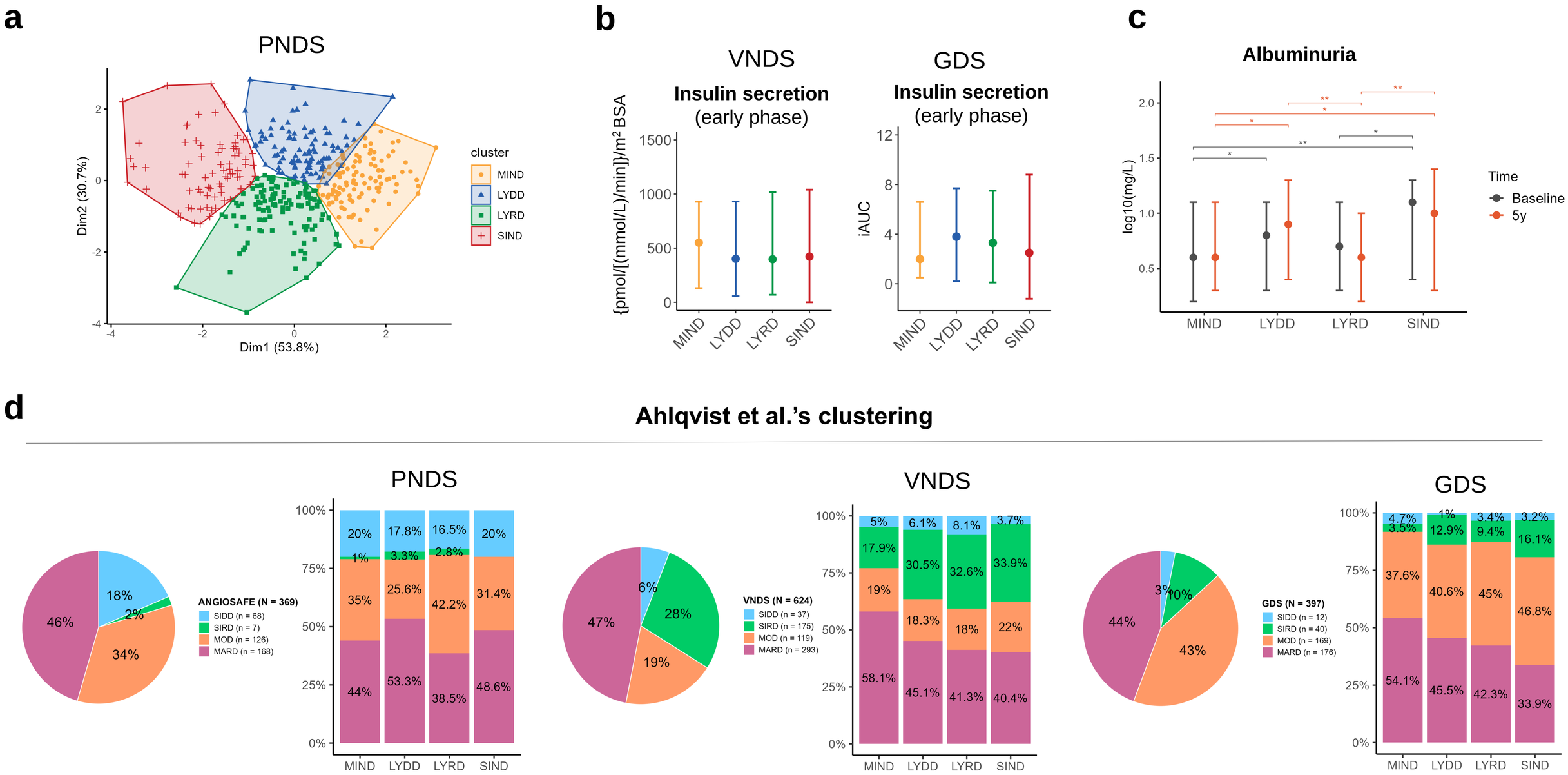

Extended Data Fig. 1: Characteristics of four endotypes in newly-diagnosed T2D cohorts (related to Fig. 2)
a, UMAP showing four endotypes identified by k-mean clustering in the PNDS discovery cohort. **b,** Early-phase insulin secretion of endotypes in the VNDS and GDS cohort. **c,** Renal functions (albuminuria) across endotypes at diagnosis and 5-year follow-up in the GDS cohort. **d,** Distribution of Ahlqvist's clusters across the immune-based endotypes in the PNDS, VNDS, and GDS cohort. In the line plots, dots represent median values and error bars indicate the interquartile range (Q1, Q3). Pairwise comparisons between endotypes were performed using Dunn's test.

a

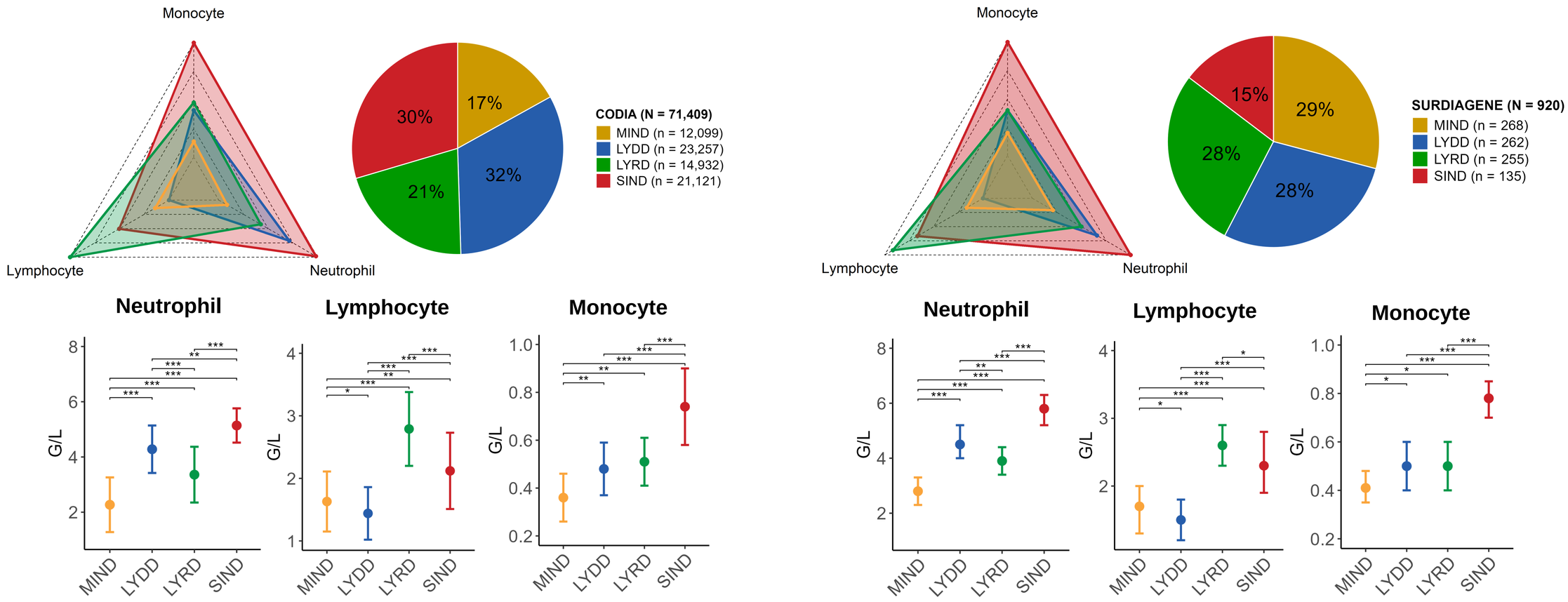

b

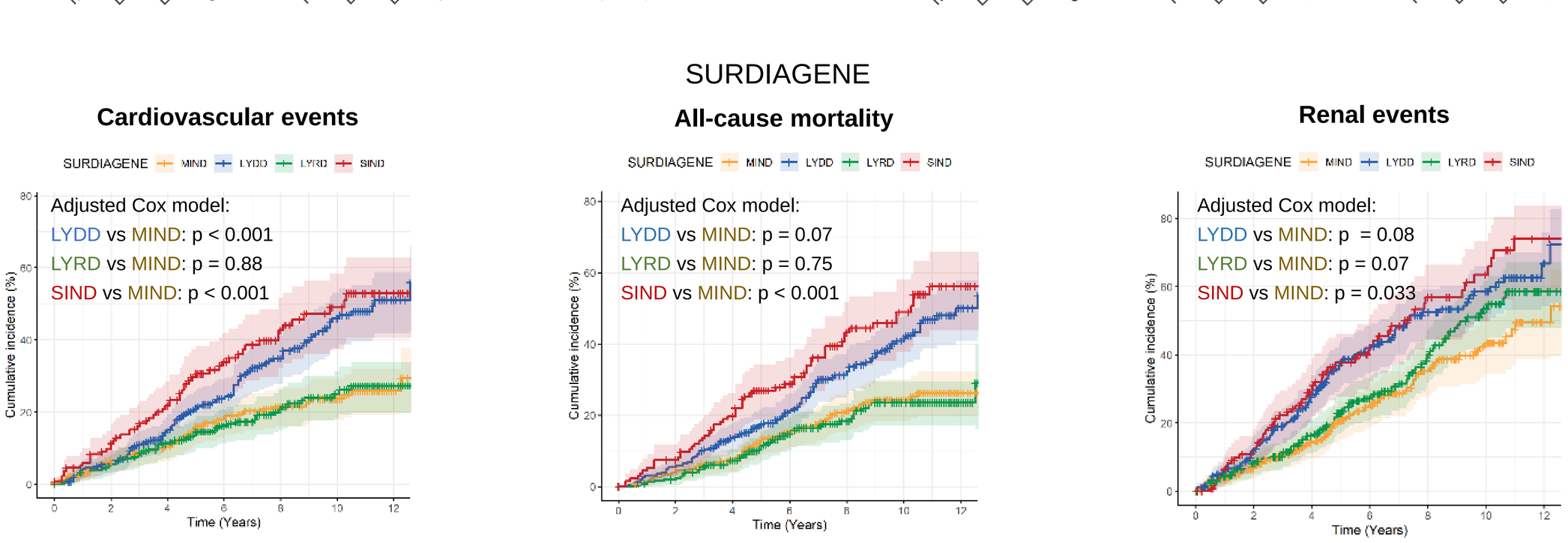

Extended Data Fig. 2: Longitudinal stability of circulating immune cell counts across endotypes and their trajectories toward T2D-related complications (related to Fig. 3)

a, Distribution of endotypes and their immune profiles across the CODIA and SURDIAGENE cohorts. **b,** Cumulative incidence of cardiovascular events, all-cause mortality, and renal events across endotypes in the SURDIAGENE and ANGIOSAFE cohort. In the radar plots, dots indicate median values of immune cell counts. In the line plots, dots represent median values and error bars indicate the interquartile range (Q1, Q3). Pairwise comparisons between endotypes were performed using Dunn's test.

a

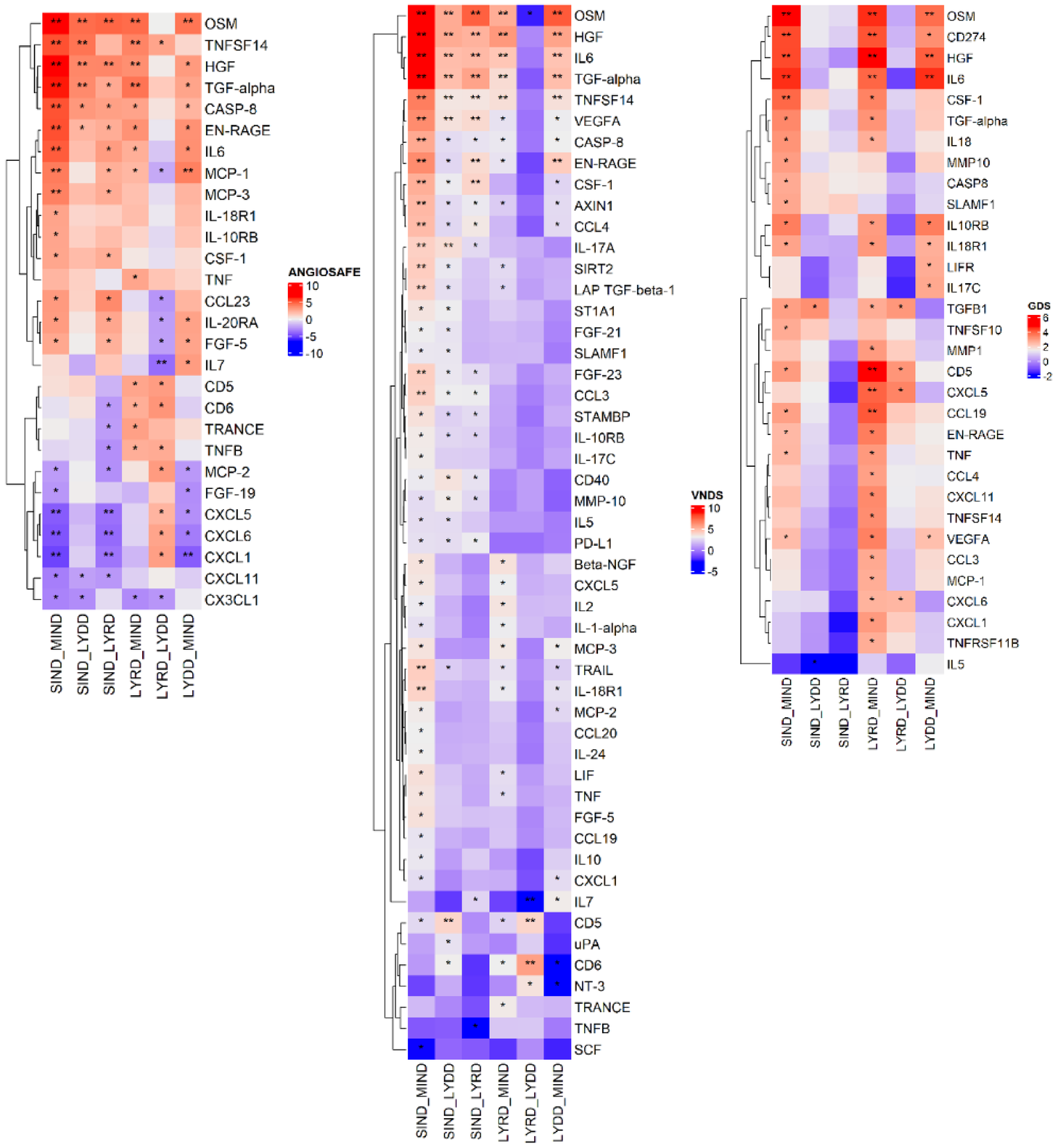
PNDS
VNDS
GDS
ANGIOSAFE
VNDS
GDS
SIND_MIND
SIND_LYDD
SIND_LYRD
LYRD_MIND
LYRD_LYDD
LYDD_MIND

b

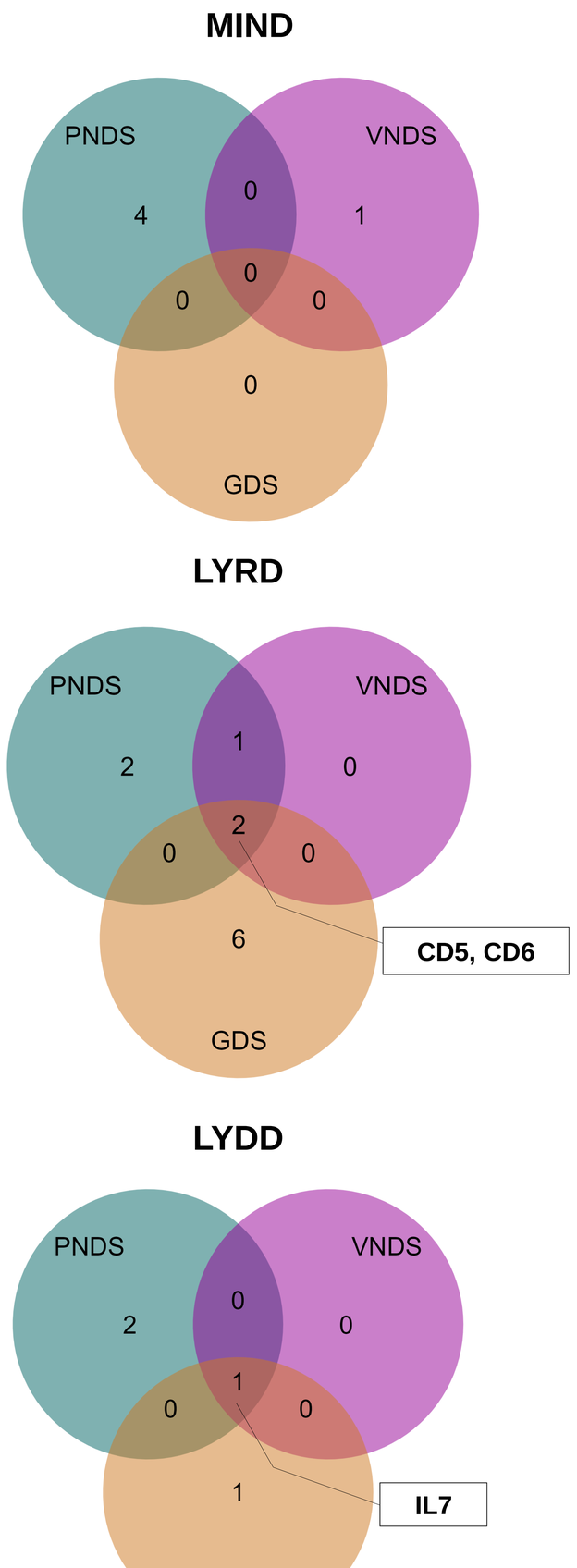
MIND
PNDS
VNDS
GDS
4
0
1
0
0
0
0
LYRD
PNDS
VNDS
GDS
2
1
0
2
0
0
6
CD5, CD6
LYDD
PNDS
VNDS
GDS
2
0
0
1
0
0
1
IL7

c

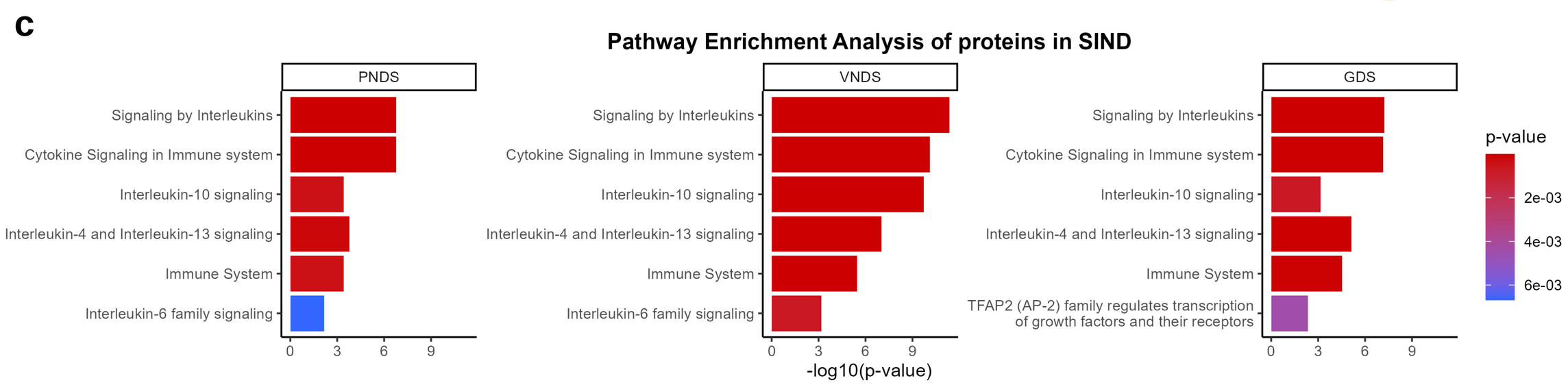
Pathway Enrichment Analysis of proteins in SIND
PNDS
VNDS
GDS
Signaling by Interleukins
Cytokine Signaling in Immune system
Interleukin-10 signaling
Interleukin-4 and Interleukin-13 signaling
Immune System
Interleukin-6 family signaling
TFAP2 (AP-2) family regulates transcription of growth factors and their receptors
0
3
6
9
-log10(p-value)
p-value
2e-03
4e-03
6e-03

d

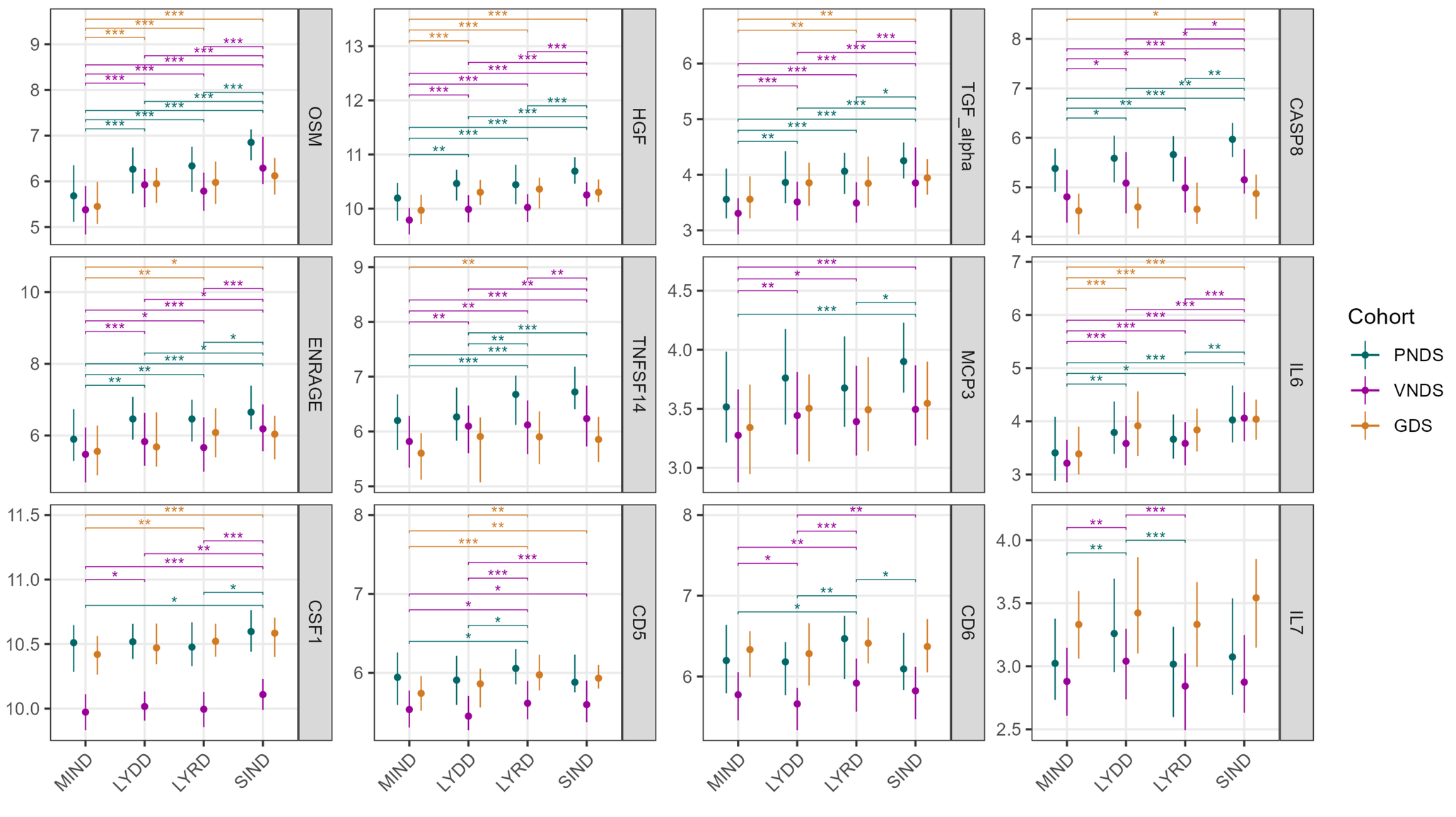
OSM
HGF
TGF_alpha
CASP8
ENRAGE
TNFSF14
MCP3
IL6
CSF1
CD5
CD6
IL7
MIND
LYDD
LYRD
SIND
Cohort
PNDS
VNDS
GDS

Extended Data Fig. 3: Inflammation-related proteomic signatures of T2D endotypes across cohorts (related to Fig. 4)

a, Pairwise comparisons of proteins with at least one significant pairwise difference in PNDS (n = 384), VNDS (n = 660), and GDS cohort (n = 354). Heatmaps show the mean rank differences in pairwise comparisons of the Dunn test and corresponding P values in asterisks **b,** Common proteins enriched in MIND, LYRD, and LYDD across the cohorts. **c,** Pathway enrichment analysis of endotype-enriched proteins in SIND across PNDS, VNDS and GDS cohort. **d,** Levels of endotype-enriched proteins across endotypes in three cohorts. In the line plots, dots represent median values and error bars indicate the interquartile range (Q1, Q3). Pairwise comparisons between endotypes were performed using Dunn’s test.

a

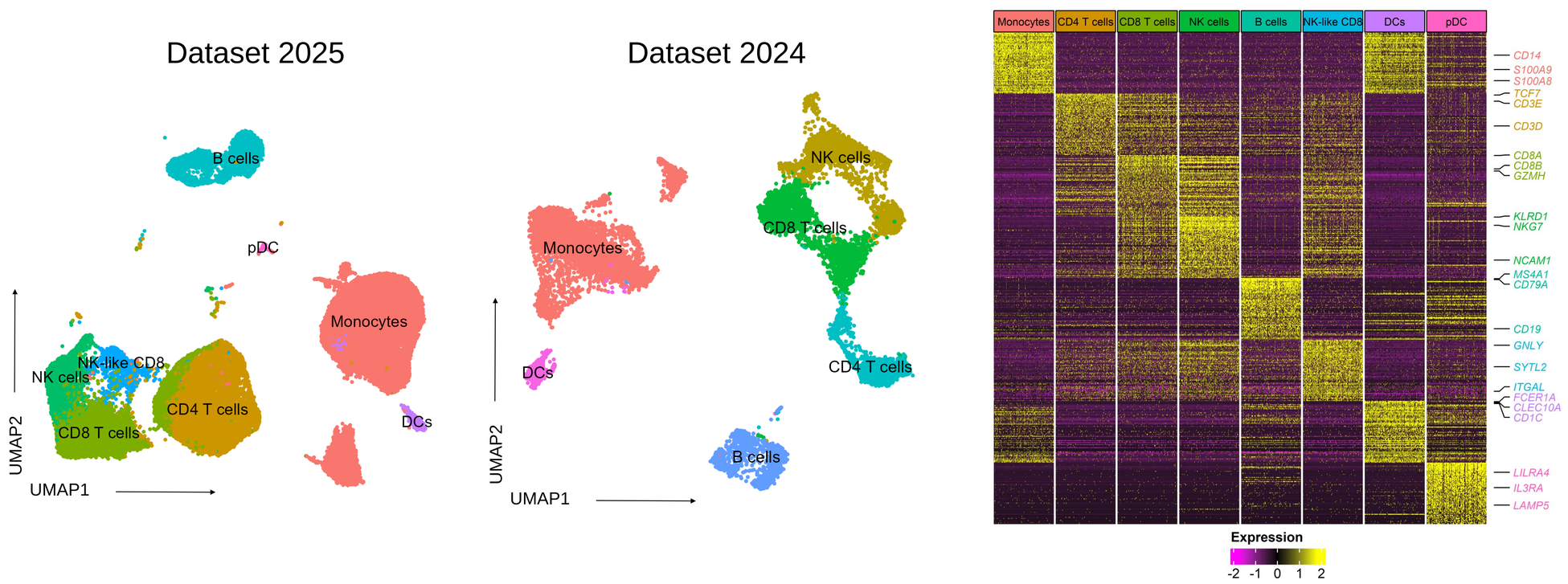

b

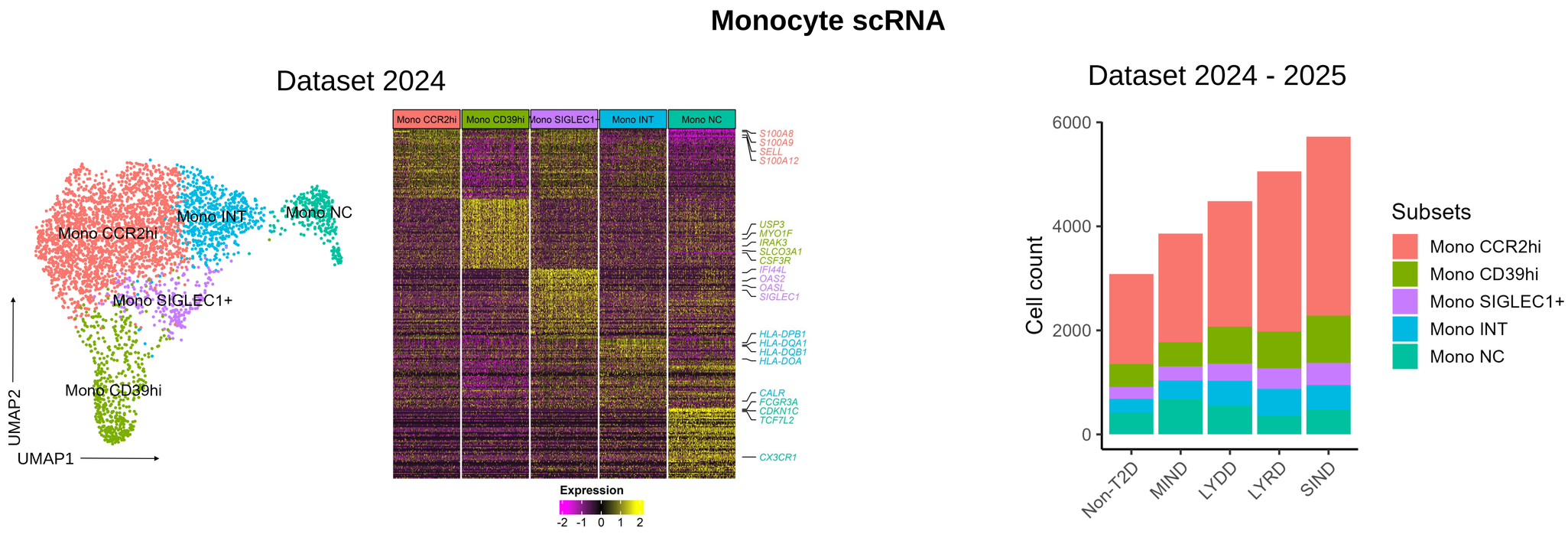

c

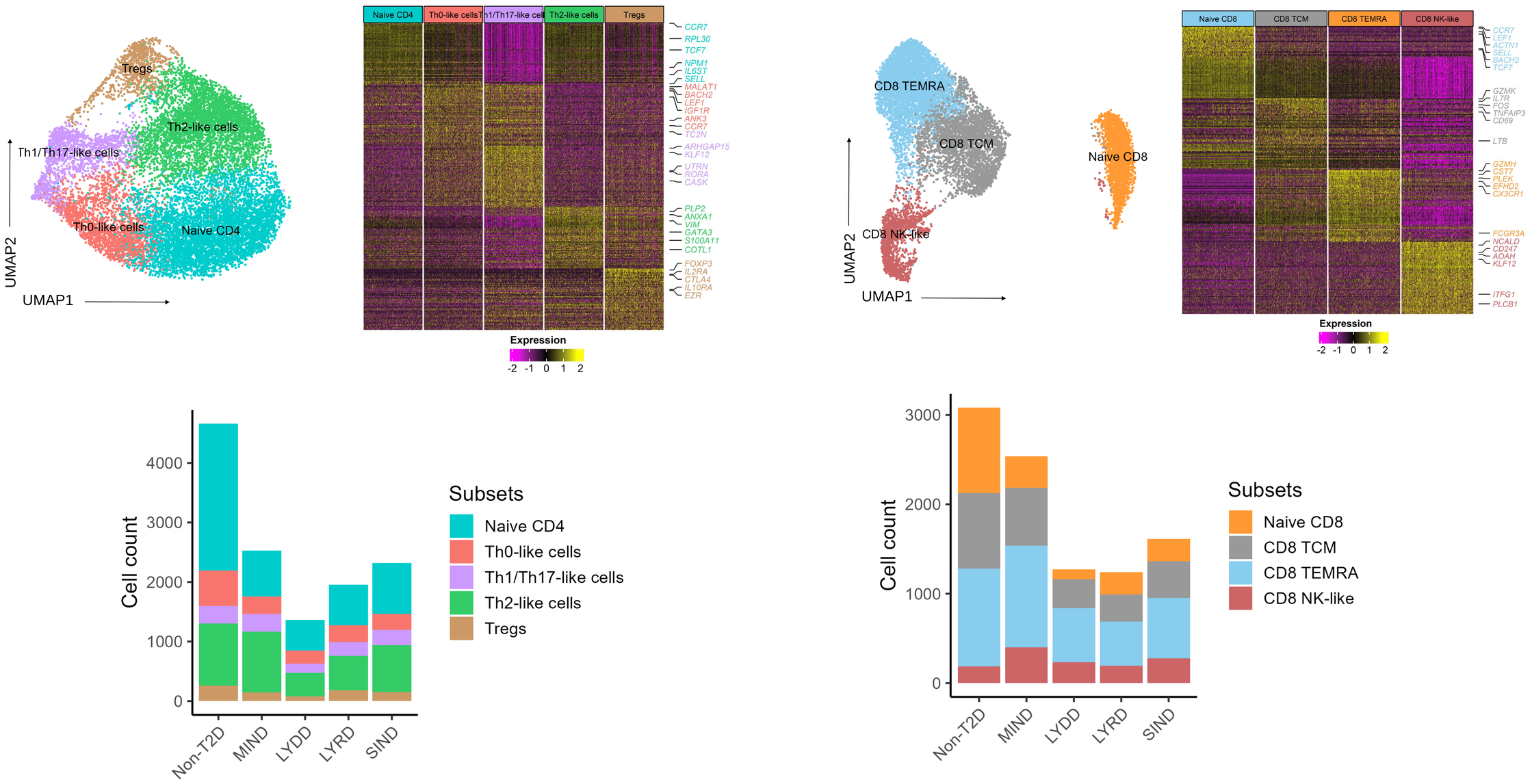

Extended Data Fig. 4: Single-cell RNA-sequencing of PBMCs revealing monocyte and lymphocyte composition across endotypes (related to Fig. 5)

a, UMAP visualization of PBMC subpopulations derived from scRNA-seq, with heatmap of top marker genes. **b,** UMAP visualization of monocyte subsets derived from scRNA-seq, with heatmap of top marker genes (**left**). Monocyte subset counts in non-T2D group and T2D endotypes (**right**). **c,** UMAP visualization of $CD4^+$ and $CD8^+$ lymphocyte subsets derived from scRNA-seq; heatmap of top marker genes; $CD4^+$ and $CD8^+$ lymphocyte subset counts in non-T2D group and T2D endotypes.

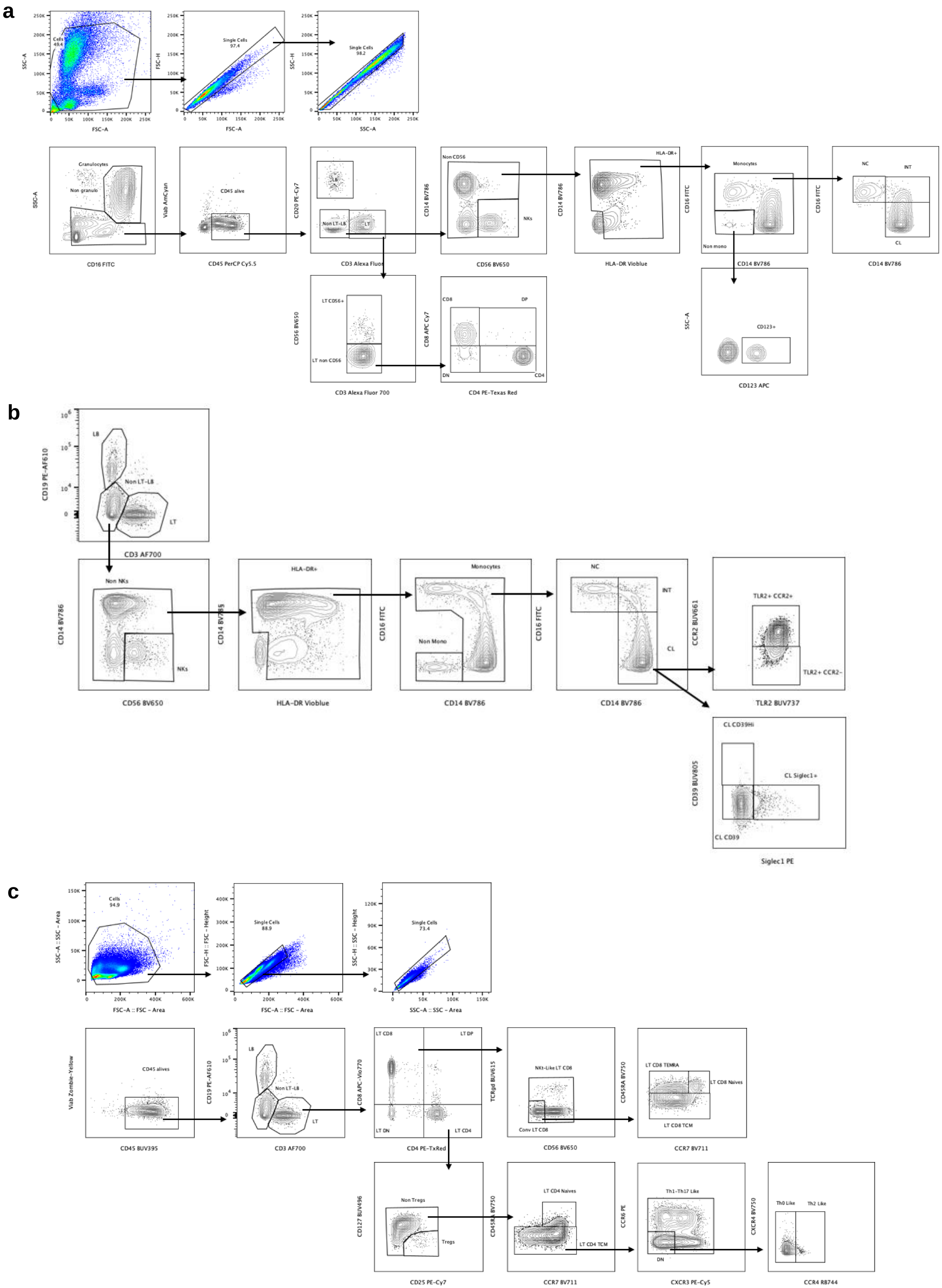

Extended Data Fig. 5: Flow cytometry gating strategy (related to Fig. 5)

a-c, Gating strategy identifying PBMC subpopulations (**a**), monocyte subsets (**b**), and lymphocyte subsets (**c**).

a

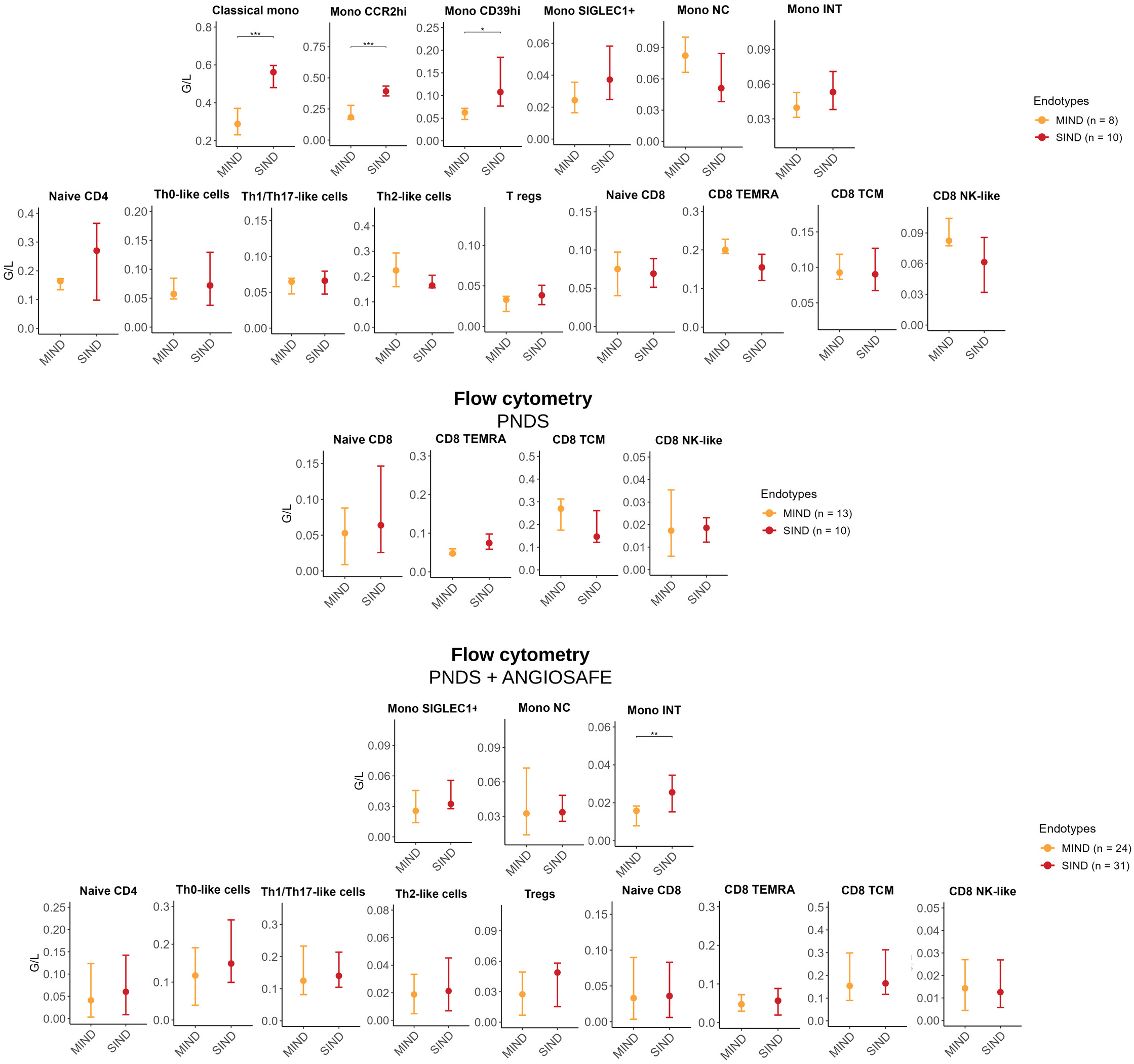
scRNA
PNDS
Classical mono
Mono CCR2hi
Mono CD39hi
Mono SIGLEC1+
Mono NC
Mono INT
Naive CD4
Th0-like cells
Th1/Th17-like cells
Th2-like cells
T regs
Naive CD8
CD8 TEMRA
CD8 TCM
CD8 NK-like
G/L
MIND
SIND
Endotypes
MIND (n = 8)
SIND (n = 10)
Flow cytometry
PNDS
Naive CD8
CD8 TEMRA
CD8 TCM
CD8 NK-like
Endotypes
MIND (n = 13)
SIND (n = 10)
Flow cytometry
PNDS + ANGIOSAFE
Mono SIGLEC1+
Mono NC
Mono INT
Endotypes
MIND (n = 24)
SIND (n = 31)
Naive CD4
Th0-like cells
Th1/Th17-like cells
Th2-like cells
Tregs
Naive CD8
CD8 TEMRA
CD8 TCM
CD8 NK-like

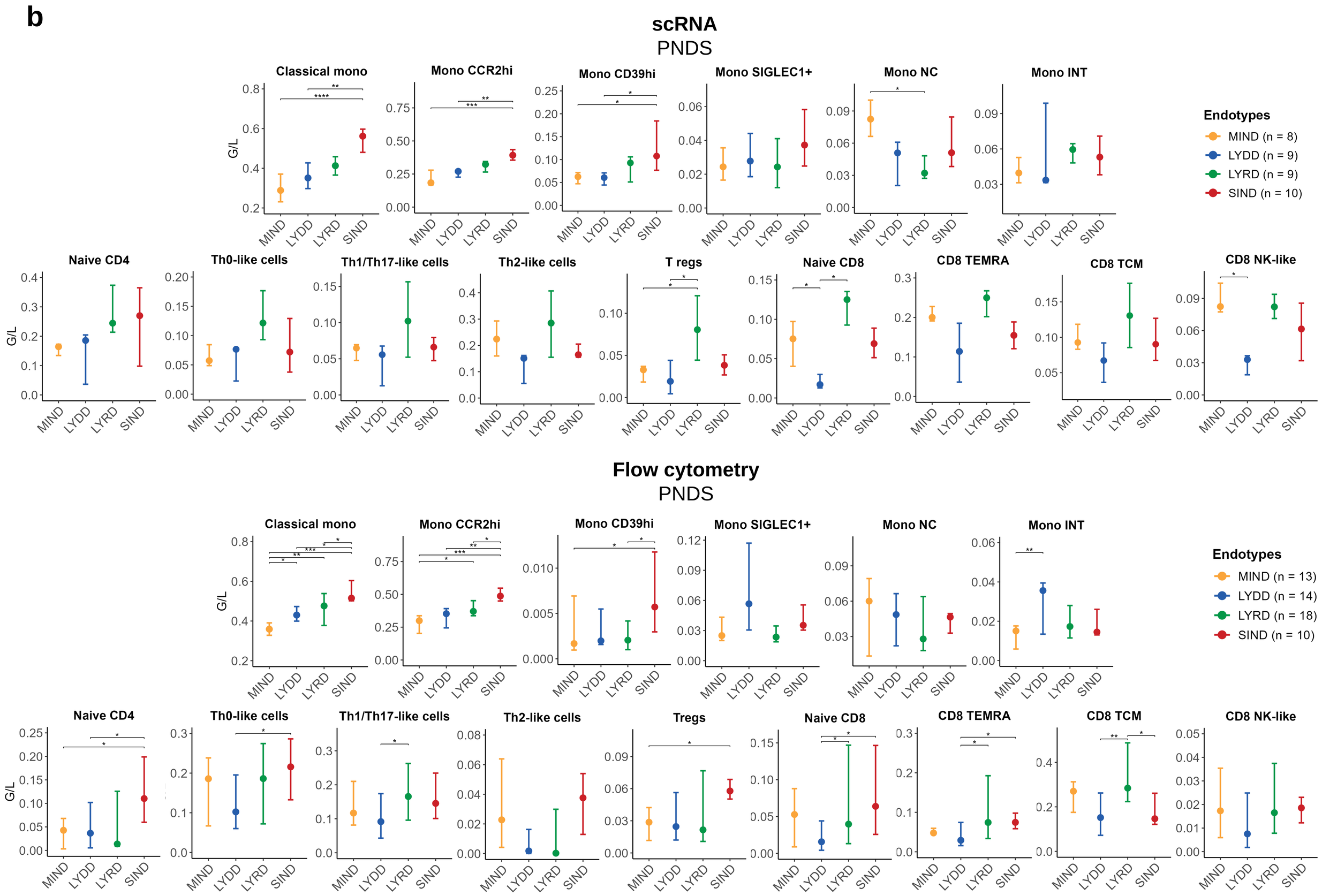

Extended Data Fig. 6: Monocyte and lymphocyte subset counts across T2D endotypes from single-cell RNA-sequencing and flow cytometry (related to Fig. 5)

a-b Monocyte and lymphocyte subset counts derived from scRNA-seq data and flow cytometry in SIND and MIND (**a**), and across four endotypes (**b**). **c,** UMAP plot of monocyte and lymphocyte subsets identified by flow cytometry of non-T2D groups. **d,** Enriched pathways of Mono CCRhi and Mono CD39hi (scRNA-seq). In the line plots, dots represent median values and error bars indicate the interquartile range (Q1, Q3). Pairwise comparisons between endotypes were performed using Dunn's test. Comparisons between SIND and MIND were performed using Mann–Whitney U test.

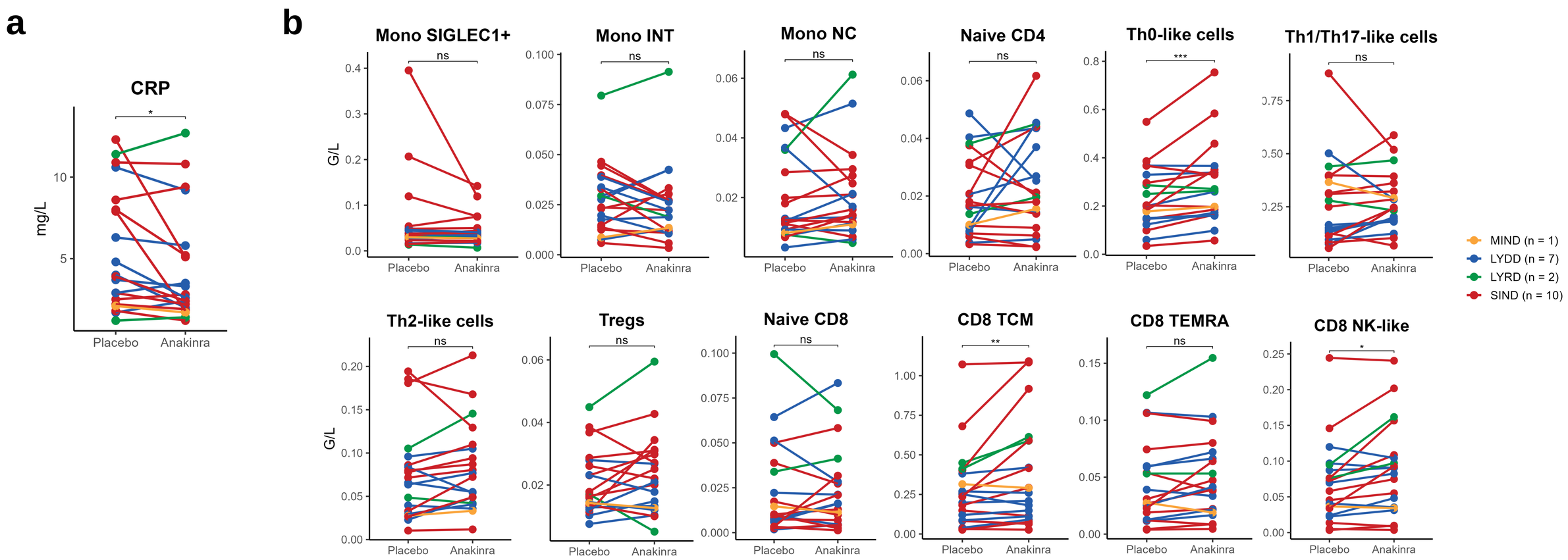

Extended Data Fig. 7: Monocyte and lymphocyte subset counts in Hyper-preDIL Study (related to Fig. 6)
a-b, Changes in CRP (**a**), monocyte and lymphocyte subset counts (**b**) following placebo and anakinra treatment. In the line graphs, each line represents a paired value of one individual. Paired comparisons were assessed using the Wilcoxon signed-rank test.